Ising order in a magnetized Heisenberg chain subject to a uniform Dzyaloshinskii-Moriya interaction

Yang-Hao Chan, Wen Jin, Hong-Chen Jiang, and Oleg A. Starykh

Phys. Rev. B **96**, 214441 — Published 29 December 2017

DOI: 10.1103/PhysRevB.96.214441

Ising orders in a magnetized Heisenberg chain subject to a uniform Dzyaloshinskii-Moriya interaction

Yang-Hao Chan,[1] Wen Jin,[2] Hong-Chen Jiang,[3] and Oleg A. Starykh[2]

[1]*Institute of Atomic and Molecular Sciences, Academia Sinica, Taipei 10617, Taiwan*
[2]*Department of Physics and Astronomy, University of Utah, Salt Lake City, Utah 84112, USA*
[3]*Stanford Institute for Materials and Energy Sciences, SLAC National Accelerator Laboratory and Stanford University, 2575 Sand Hill Road, Menlo Park, CA 94025, USA*

(Dated: December 13, 2017)

We report combined analytical and density matrix renormalized group (DMRG) study of the antiferromagnetic XXZ spin-1/2 Heisenberg chain subject to a uniform Dzyaloshinskii-Moriya (DM) interaction and a transverse magnetic field. The numerically determined phase diagram of this model, which features two ordered Ising phases and a critical Luttinger liquid one with fully broken spin-rotational symmetry, agrees well with the predictions of Garate and Affleck [Phys. Rev. B 81, 144419 (2010)]. We also confirm the prevalence of the "N^z" Néel Ising order in the regime of comparable DM and magnetic field magnitudes.

PACS numbers:

I. INTRODUCTION

Physics of quantum spins is at the center of modern condensed matter research. The ever present spin-orbit interactions, long considered to be an unfortunate annoying feature of real-world materials, are now recognized as the key ingredient of numerous spintronics applications[1,2] and the crucial tool for constructing topological phases[3,4].

In magnetic insulators atomic spin-orbit coupling leads, via superexchange mechanism, to an asymmetric spin exchange $\mathbf{D}_{ij} \cdot \mathbf{S}_i \times \mathbf{S}_j$, known as Dzyaloshinskii-Moriya (DM) interaction[5,6], between localized spins $\mathbf{S}$ at sites i and j. Classically, such an interaction induces incommensurate spiral correlations in the plane perpendicular to the DM vector $\mathbf{D}_{ij}$. Incommensurability of the spin spiral is determined by D/J, where J is the magnitude of the isotropic exchange interaction between nearest spins. This ratio is typically quite small, resulting in spiral correlations with very long wavelengths. It was realized long ago that the external magnetic field, applied *perpendicular* to the DM axis, causes strong modification of the spiral state and produces chiral soliton lattice - a periodic array of commensurate with the lattice domains separated by 2π-domain walls (solitons)[7]. This incommensurate structure undergoes continuous incommensurate-commensurate transition into a uniform ordered state at a rather small critical magnetic field of the order of D.[7–9] Such potential tunability makes this interesting class of magnetically-ordered materials particularly attractive for multiferroics and spintronics applications[10,11].

It is not well understood how strong quantum fluctuations modify this classical picture. To this end, and also having in mind several spin-1/2 quasi-one-dimensional quantum magnets[12–14] for which this consideration is highly relevant, we investigate here the joint effect of a uniform DM interaction $D\hat{z} \cdot \mathbf{S}_i \times \mathbf{S}_{i+1}$ and a transverse magnetic field hS_i^x on the low-energy properties of the antiferromagnetic spin-1/2 Heisenberg chain with a weak XXZ anisotropy Δ. Our goal is to quantitatively check, with the help of the state of the art density-matrix renormalization group (DMRG) calculation, predictions of the recent field-theoretic studies of this interesting problem[15–17]. Garate and Affleck, Ref. 16, found that quantum fluctuations destroy the chiral soliton lattice and replace it with a critical Luttinger-liquid (LL) phase. Additionally, the model is found to support two distinct ordered phases with staggered Ising order along directions perpendicular to the external field $\mathbf{h}$. Regions of stability of these Ising phases are found to differ significantly from the classical expectations[15,16]. In particular, when the magnitudes of DM interaction D and magnetic field h are comparable to each other, the Ising-like longitudinal spin-density wave order (of "N^z" kind, see below) is found to extend deep into classically forbidden $\Delta \leq 1$ region.

The outline of the paper is as follows. Sec. II reviews the field-theory arguments and Sec. III summarizes the quantum phase diagram. Main DMRG results are presented in Sec IV, while Sec. V focuses on understanding of the strong finite-size effects observed in our study. Numerous Appendices provide technical details of our analytical (A through E) and numerical (F) calculations.

II. HAMILTONIAN OF THE MODEL

We consider antiferromagnetic Heisenberg spin-1/2 chains subject to a uniform Dzyaloshinskii-Moriya (DM) interaction and a transverse external magnetic field. The

system is described by the following Hamiltonian,

$$\mathcal{H} = J\sum_i \left[S_i^x S_{i+1}^x + S_i^y S_{i+1}^y + \Delta S_i^z S_{i+1}^z\right] - \sum_i D\hat{z}\cdot(\boldsymbol{S}_i \times \boldsymbol{S}_{i+1}) - h\sum_i S_i^x, \quad (1)$$

where $\mathbf{S}_i$ is the spin-1/2 operator at site i. J denotes antiferromagnetic exchange coupling between nearest neighbors (NN). $\Delta \approx 1$ parameterizes small Ising anisotropy. Dzyaloshinskii-Moriya (DM) interaction is parameterized by the DM vector $\mathbf{D} = D\hat{z}$, which is uniform along the chain. We consider $D/J \ll 1$, which is the most natural limit relevant for real materials[12–14,18]. In addition to 'twisting' spins around the $\boldsymbol{D}$ axis, the uniform DM interaction slightly renormalizes Ising anisotropy[16] by an amount $\propto D^2/J^2$. h denotes the strength of the applied transverse magnetic field.

A. Hamiltonian in the low-energy limit

In the low-energy continuum limit, the bosonized Hamiltonian of the problem reads[15,16,19],

$$\mathcal{H}_{\rm chain} = \tilde{H}_0 + \tilde{H}_{\rm bs}, \quad (2)$$

where $\tilde{H}_0$ has quadratic form in terms of abelian bosonic fields (φ, ϑ) [see Appendix A for details], and the Zeeman and DM interaction terms (second line in Eq. (1)) are absorbed in $\tilde{\mathcal{H}}_0$ by a chiral rotation and subsequent linear shift of field φ as described in Appendix B. The harmonic Hamiltonian $\tilde{H}_0$ is perturbed by the chain backscattering $\tilde{H}_{\rm bs}$ describing residual backscattering interaction between right- and left-moving spin modes of the chain. It consists of several contributions[15,16,20]

$$\begin{aligned}
\tilde{H}_{\rm bs} &= H_A + H_B + H_C + H_\sigma,\\
H_A &= \pi v y_A \int {\rm d}x (M_R^z M_L^+ e^{it_\varphi x} - M_R^+ M_L^z e^{-it_\varphi x} + {\rm h.c.}),\\
H_B &= \pi v y_B \int {\rm d}x (M_R^+ M_L^- e^{-i2t_\varphi x} + {\rm h.c.}),\\
H_C &= \pi v y_C \int {\rm d}x (M_R^+ M_L^+ + {\rm h.c.}),\\
H_\sigma &= -2\pi v y_\sigma \int {\rm d}x M_R^z M_L^z.
\end{aligned} \quad (3)$$

Here $\mathbf{M}_L(x)$ and $\mathbf{M}_R(x)$ are the uniform left- and right-moving spin current operators defined in Appendix B, and we use the following notations

$$y_C \equiv \frac{1}{2}(y_x - y_y), \quad y_B \equiv \frac{1}{2}(y_x + y_y), \quad y_\sigma \equiv -y_z, \quad t_\varphi \equiv \frac{\sqrt{D^2+h^2}}{v}. \quad (4)$$

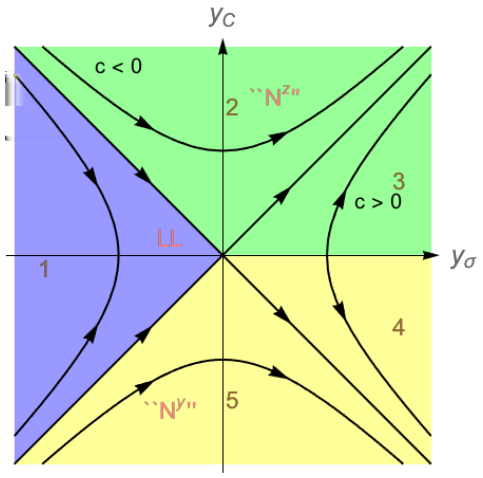

FIG. 1: (Color online) Solution of Kosterlitz-Thouless (KT) equations (11). Different symbols and colors depict Ising phases "N^z" (green region) and "N^y" (yellow region) and the critical Luttinger liquid phase (LL, purple region) according to the RG flow criteria summarized in Table I.

Initial values of the coupling constants are given by[16,20]

$$\begin{aligned}
y_x(0) &= -\frac{g_{\rm bs}}{2\pi v}[(1+\frac{\lambda}{2})\cos\theta^- + \frac{\lambda}{2}],\\
y_y(0) &= -\frac{g_{\rm bs}}{2\pi v},\\
y_z(0) &= -\frac{g_{\rm bs}}{2\pi v}[(1+\frac{\lambda}{2})\cos\theta^- - \frac{\lambda}{2}],\\
y_A(0) &= \frac{g_{\rm bs}}{2\pi v}(1+\frac{\lambda}{2})\sin\theta^-,
\end{aligned} \quad (5)$$

where the magnitude of backscattering $g_{\rm bs} \approx 0.23 \times (2\pi v)$, see Ref. 16 for details, and

$$\theta^- = 2\theta_0, \quad \theta_0 = -\arctan(D/h), \quad (6)$$

$v \simeq J\pi a/2$ is the spin velocity, a is lattice constant.

XXZ anisotropy is parameterized by λ[16],

$$\lambda = c(1 - \Delta + \frac{D^2}{2J^2}). \quad (7)$$

The constant $c = (4v/g_{\rm bs})^2$ is about 7.66 from the Bethe-ansatz solution; see (B2) in Ref. 16. The oscillating factor $e^{it_\varphi x}$ in (3) is introduced by the effective transverse field $h_{\rm eff} = \sqrt{h^2+D^2}$ which accounts for the combined effect of magnetic field and DM interaction; see (B4).

Our task is to identify the most relevant coupling in perturbation (3), which is accomplished by the renormalization group (RG) analysis.

B. Two-stage RG

RG equations for coupling constants of backscattering interaction (3) are obtained with the help of operator

Region	1	2	3	4	5
$y_C(0)$	$+/-$	$+$	$+$	$-$	$-$
$y_\sigma(0)$	$-$	$-/+$	$+$	$+$	$-/+$
C	$+$	$-$	$+$	$+$	$-$
$y_C(\ell^*)$	0	$+\infty$	$+\infty$	$-\infty$	$-\infty$
$y_\sigma(\ell^*)$	finite	$+\infty$	$+\infty$	$+\infty$	$+\infty$
$y_B(\ell^*)$	finite	finite	finite	finite	finite
State	LL	"N^z"	"N^z"	"N^y"	"N^y"

TABLE I: Signs and values of y_C, y_σ, C corresponding the KT-flow in Fig. 1. ℓ^* is the critical RG scale at which one (or several) coupling constants reach the strong coupling limit (become of order one).

product expansion (OPE[21,22]) technique and read

$$\begin{aligned} \frac{dy_x}{dl} &= y_y y_z, \quad \frac{dy_y}{dl} = y_x y_z + y_A^2, \\ \frac{dy_z}{dl} &= y_x y_y, \quad \frac{dy_A}{dl} = y_y y_A. \end{aligned} \tag{8}$$

The presence of oscillating $e^{it_\varphi x}$ factors implies the appearance of spatial scale, $\propto 1/t_\varphi$, and, correspondingly, of the RG scale ℓ_φ

$$\ell_\varphi = \log(\frac{1}{a_0 t_\varphi}) = \ln[\frac{1}{20.4}\frac{\pi}{2}\frac{1}{\sqrt{D^2+h^2}}]. \tag{9}$$

where, $a_0 = 20.4a$ is the ultraviolet RG cutoff length scale[16] (see Ref. 16 for details of how the choice of the initial value for $g_{\rm bs}$ determines a_0 also).

For $\ell < \ell_\varphi$ oscillations due to $e^{it_\varphi x}$ can be neglected and the full set of RG equations (8) has to be solved numerically. Once RG "time" $\ell > \ell_\varphi$, strong oscillations in H_A and H_B result in disappearance of these terms from the Hamiltonian. Correspondingly, we can set $y_A(\ell) = 0$ and $y_B(\ell) = 0$ in the RG equations. Therefore, at this second stage, the RG equations simplify to (see Eq. (4))

$$\frac{dy_C}{d\ell} = y_C y_\sigma, \quad \frac{dy_\sigma}{d\ell} = y_C^2. \tag{10}$$

These are the well-known Kosterlitz-Thouless (KT) equations, the analytic solution of which is summarized in Appendix C. The initial values of backscattering couplings at the second stage are,

$$\begin{aligned} y_C(\ell_\varphi) &= (y_x(\ell_\varphi) - y_y(\ell_\varphi))/2 \\ &\to -\frac{g_{\rm bs}}{4\pi v}[(1+\frac{\lambda}{2})\cos\theta^- - 1 + \frac{\lambda}{2}], \\ y_\sigma(\ell_\varphi) &= -y_z(\ell_\varphi) \to \frac{g_{\rm bs}}{2\pi v}[(1+\frac{\lambda}{2})\cos\theta^- - \frac{\lambda}{2}], \\ C &= y_\sigma(\ell_\varphi)^2 - y_C(\ell_\varphi)^2, \end{aligned} \tag{11}$$

where $\cos\theta^- = (h^2 - D^2)/(h^2 + D^2)$ and C is the constant of motion, $dC/d\ell = 0$. Expressions following right-arrow sign, $\to$, in the above equations pertain to the situation when the first stage of RG flow, $\ell < \ell_\varphi$, can be skipped. This is the case of strongly oscillating $e^{it_\varphi x}$ factors in Eq. (3), when all the oscillating terms in the backscattering Hamiltonian can be omitted from the outset and, correspondingly, $y_a(\ell_\varphi) \approx y_a(0)$. Formally, this limit corresponds to a *negative* ℓ_φ as defined in Eq. (9).

C. Ising orders

We have identified five distinct regions with different signs of $y_{C,\sigma}$ and integration constant C, which result in different RG flows. The boundaries of these regions depend on the initial values of y's and C. When the first-stage flow can be skipped, which happens for sufficiently large $h_{\rm eff}$ such that formally $\ell_\varphi < 0$, as discussed at the end of Sec. II B, then the dependence on initial values can be directly translated into that on h/D ($\cos\theta^-$) and λ (Δ and D/J). These results are summarized in Table I and Fig. 1, which shows what orders are promoted in different regions.

Small t_φ results in $\ell_\varphi > 0$ and a two-step RG analysis is required, as explained above. Once the RG equations (8) are integrated to $\ell = \ell_\varphi$, all the oscillating terms must be dropped and only two momentum-conserving terms, H_c and H_σ, remain present in the Hamiltonian.

In terms of abelian fields (φ, ϑ), interaction H_C is nonlinear, $H_C \propto y_C \cos[2\sqrt{2\pi}\vartheta] = y_C \cos[2\beta\vartheta]$, while $H_\sigma \propto (\partial_x\varphi)^2 - (\partial_x\vartheta)^2$ and describes renormalization of β, see Appendix E 1. (We neglect marginal renormalization of the spinon's velocity $v \to v\sqrt{1 - y_\sigma^2/2}$.) The ground state of the chain is determined by the ordering of ϑ field.

It is important to understand how the chiral rotation, which led to (3), affects staggered magnetization and dimerization. Arguments in Appendix B show that staggered magnetization $\mathbf{N}$ and dimerization ϵ in the laboratory frame are related to those in the rotated frame, $\boldsymbol{\mathcal{N}}$ and ξ, as follows:

$$\begin{aligned} \boldsymbol{N} &= (-\mathcal{N}^z, \cos\theta_0 \mathcal{N}^y + \sin\theta_0 \xi, \mathcal{N}^x), \\ \epsilon &= \cos\theta_0 \xi - \sin\theta_0 \mathcal{N}^y. \end{aligned} \tag{12}$$

Further, shift of φ field by $t_\varphi x$, Eq. (B9), introduces $t_\varphi x$ dependence in arguments of fields $\mathcal{N}^z$ and ξ, Eq. (B11), but does not affect $\mathcal{N}^{x,y}$ pair.

Flow of the KT equations (10) to strong-coupling implies development of the expectation value for ϑ field. When $y_C \to +\infty$ for $\ell \to \infty$, the energy is minimized by $\sqrt{2\pi}\vartheta = (2k_1+1)\pi/2$, with k_1 an integer, and $\mathcal{N}^x \propto -\sin\sqrt{2\pi}\vartheta \neq 0$. This means that in the original frame there is an Ising order $N^z \neq 0$, and following Ref. 16 we name this state "N^z". The long-range order (staggered magnetization) in the laboratory frame is *commensurate*,

$$\langle \boldsymbol{N}(x) \rangle \propto \langle \sin(\sqrt{2\pi}\vartheta) \rangle \mathbf{z} \propto (-1)^{k_1+1}\mathbf{z}. \tag{13}$$

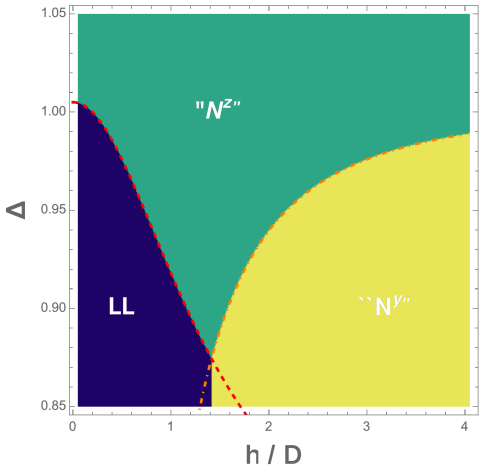

FIG. 2: (Color online) Phase diagram for the case of relatively strong DM interaction $D/J = 0.1$. Larger D promotes "N^z" state. The two phase boundaries are given by Eq. (15) (orange dot-dashed line), and Eq. (16) (red dashed line). The phase boundary between LL and "N^y" is located at $h/D = \sqrt{2}$ and is independent of Δ.

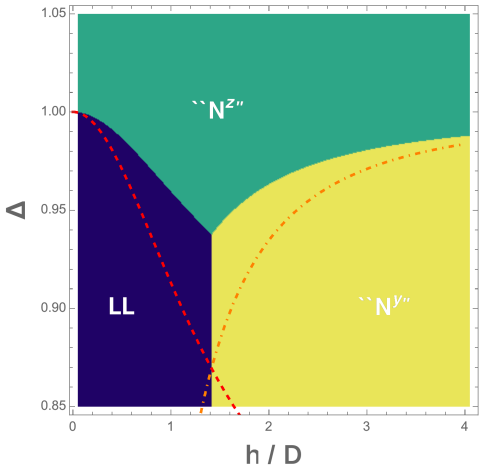

FIG. 3: (Color online) Phase diagram for the case of small DM interaction $D/J = 0.01$ obtained via a two-stage RG process. At the first stage RG equations (8) are integrated numerically. Second stage equations (10) are then solved analytically. The phase boundaries given by Eq. (15) (orange dot-dashed line) and Eq. (16) (red dashed line) are seen to deviate significantly from the actual ones. This shows the importance of the first-stage flow in the case of small and intermediate D/J.

In the case of $y_C \to -\infty$ the energy is minimized by $\sqrt{2\pi}\vartheta = k_2\pi$, with k_2 an integer, and $\mathcal{N}^y \propto \cos\sqrt{2\pi}\vartheta \neq 0$. Therefore the Ising order is now along the $\mathbf{y}$ axis, $N^y \neq 0$, and we name it "N^y". In addition, according to Eq. (12) finite expectation value of $\mathcal{N}^y$ implies finite staggered magnetization ϵ.[16] Therefore "N^y" phase is characterized by the coexistence of *commensurate* Ising Néel and dimerization orders

$$\begin{aligned}\langle \boldsymbol{N}(x)\rangle &\propto \cos\theta_0\langle\cos(\sqrt{2\pi}\vartheta)\rangle\mathbf{y} \propto \cos\theta_0(-1)^{k_2}\mathbf{y},\\ \epsilon &\propto -\sin\theta_0\langle\cos(\sqrt{2\pi}\vartheta)\rangle \propto \sin\theta_0(-1)^{k_2+1}.\end{aligned} \tag{14}$$

Finally, a gapless regime of $y_C \to 0$ for $\ell \to \infty$ is also possible[16]. Here the Hamiltonian is purely quadratic and describes a critical Luttinger liquid (LL) phase with algebraic correlations even though the spin rotational symmetry is fully broken[16,23]; see Appendix E 3 for detailed arguments. As described in the Introduction, LL state is the quantum version of the classical chiral soliton lattice phase. This is a critical state with *incommensurate* (and anisotropic) spin correlations which decay algebraically with distance.

III. PHASE DIAGRAM OF THE QUANTUM MODEL

The $\Delta - (h/D)$ phase diagrams are obtained by solving the RG equations and are presented in Figs. 2 and 3. Fig. 2 is obtained under the condition that the first-stage RG flow can be skipped, due to the fact that $\ell_\varphi < 0$ in Eq. (9) which happens for sufficiently large D and/or h. Here we choose $D/J = 0.1$. In this situation we can determine the ground state simply by studying the initial conditions of the KT equations according to the chart in Table I and Fig. 1.

When $\ell_\varphi > 0$ oscillations develop over some finite lengthscale and one needs to integrate the first-stage RG equations (8) numerically for the interval $0 \le \ell \le \ell_\varphi$. At the end of the first stage we obtain $y_C(\ell_\varphi)$, $y_\sigma(\ell_\varphi)$, and $C = y_\sigma^2(\ell_\varphi) - y_C^2(\ell_\varphi)$ which serve as initial values of the couplings for the second-stage, KT part, of the RG flow. This is the case of $D/J = 0.01$ phase diagram for which is presented in Fig. 3.

By comparing the phase diagrams in Figs. 2 and 3 we observe that large D promotes the "N^z" state, which is consistent with the numerical DMRG result in Fig. 4.

Next we study phase boundaries between different phases. Figure 1 shows that the phase transition between "N^y" and "N^z" states is related to the initial values of y_C and y_σ. The coupling $y_C(0)$ has opposite signs in the regions 3 and 4. Therefore in the $\Delta - h/D$ phase diagram this boundary corresponds a critical value Δ_{c1} at which $y_C(0) = 0$ and $C = y_\sigma^2(0) > 0$. These conditions indicate the boundary is described by $D/h = \sqrt{\lambda/2}$, which leads to the explicit expression for it:

$$\Delta_{c1} = 1 + \frac{1}{2}(\frac{D}{J})^2 - \frac{2}{c}(\frac{D}{h})^2. \tag{15}$$

For a fixed D, a larger field h leads to a greater Δ_{c1}, which is illustrated as orange dot-dashed line in Figs. 2 and 3. Figure 2 shows an excellent agreement of the obtained phase transition line with the numerical solution of RG equations, thanks to the fact that in this case the first stage of RG flow is not required. Interestingly, the limit of $D \to 0$, corresponding to $h/D \to \infty$ in the above figures, is described by our theory as well, as we explain in

Appendix D. In that case one deals with the XXZ model in the transverse magnetic field for which the critical line separating the two Ising phases, "N^y" and "N^z", is reduced to the horizontal asymptote $\Delta_{c1} = 1$, in agreement with the previous study in Ref. 24.

The boundary between gapless LL and Ising "N^z", according to Table I, happens at $C = 0$, $y_C(0) > 0$, and $y_\sigma(0) < 0$. Therefore we have the relation that $y_\sigma(0) = -y_C(0)$. This gives the critical Δ_{c2}

$$\Delta_{c2} = 1 + \frac{1}{2}(\frac{D}{J})^2 - \frac{2}{c}\frac{1}{1+2(D/h)^2}. \qquad (16)$$

Therefore, in contract to Eq. (15), a larger field h results in a smaller Δ_{c2}. This result is also confirmed in Figs. 2 and 3.

Finally, the transition between LL and Ising "N^y" is described by $C = 0$, $y_C(0) < 0$, and $y_\sigma(0) < 0$. This gives $y_C(0) = y_\sigma(0)$ which is satisfied by $\cos\theta^- = 1/3$ and $\lambda \geq 1$. This condition implies that transition between LL and "N^y" is a vertical line located at $(h/D)_{c3} = \sqrt{2}$, which is again confirmed by numerical solution of RG equations in Figs. 2 and 3. Different from the other two boundaries, the one between LL and "N^y" is independent of Δ, and this is consistent with the classical analysis in Ref. 16. The constraint $\lambda \geq 1$ implies that this boundary exists only for $\Delta \leq \Delta_t \equiv 1+(D/J)^2/2-1/c$. The crossing point of the critical lines Δ_{c1} and Δ_{c2} also gives the condition $(h/D)_{c3} = \sqrt{2}$. The "triple" point where three phases intersect is at $h/D = \sqrt{2}$ and Δ_t. For $D/J = 0.1$ in Fig. 2 it is evaluated to be at $\Delta_t \simeq 0.874$.

The main message of this Section is that strong DM interaction, acting jointly with transverse magnetic field, causes significant modification of the classical phase diagram and works to stabilize Ising "N^z" order well beyond its classical domain of stability (given by $\Delta > 1$), in agreement with the field-theoretical predictions of Refs. 15 and 16.

IV. NUMERICAL STUDIES

In this section, we will determine the ground state properties of the model system in Eq. (1) by an extensive and accurate density-matrix renormalization group (DMRG)[25–27] simulations. Here, we consider a system with total number of sites L up to $L = 1600$, and perform 10 sweeps by keeping up to $m = 400$ DMRG states with typical truncation error of the order 10^{-9}. In addition, we have also carried out an independent infinite time-evolving block decimation (iTEBD)[28–30] simulations with the same bond dimension and the same lengths for the correlation function calculations. Our iTEBD results agree fully with our DMRG results (see Fig.4 below).

Our principal results are summarized in the phase diagram in Fig.4 at $D/J = 0.05$ and $D/J = 0.1$. Changing the parameters Δ and h/D, we find three distinct phases, including a gapless Luttinger liquid (LL) phase and two ordered phases – the Néel Ising ordered "N^z" (Ising order along z-axis) and "N^y" (Ising order along y-axis) phases. Our numerical results show that the DM interaction stabilizes the "N^z" Ising order which extends into the $\Delta < 1$ region, while the "N^y" Ising order gets suppressed by the DM interaction and gives way to the LL phase for relatively small transverse magnetic field $h \lesssim D$. These results agree well with the field-theory predictions described in Secs. II and III, although with slightly different phase boundaries due to significant finite size effects which are described in more details in Sec. V.

To characterize distinct phases of the phase diagram, we measure magnetic correlations in the ground state by evaluating the equal time spin structure factor $M_s^\alpha(k) = \frac{1}{L}\sum_{ij}^{L} e^{\imath k(r_i-r_j)}\langle S_i^\alpha S_j^\alpha\rangle$, where $\alpha = x, y, z$ denotes different spin components. The structure factor is peaked at $k = \pi$ in both "N^z" and "N^y" phases, corresponding to the commensurate Néel Ising order along z-axis and y-axis, respectively. To quantitatively analyze this order, we perform an extrapolation of the spin order parameter $N^\alpha(k) = \sqrt{M_s^\alpha(k)/L}$ to the thermodynamic limit ($L = \infty$) according to the generally accepted form

$$N^\alpha(k, L) = N^\alpha(k, \infty) + \frac{a}{\sqrt{L_{1/2}}} + \frac{b}{L_{1/2}} \qquad (17)$$

where a and b are fitting parameters, see Appendix F for details. The structure factor for finite system of length L is calculated by using only the central $L_{1/2} = L/2$ part of finite systems. In addition to the spin order, we also calculate the dimer structure factor $M_d(k) = \frac{1}{L}\sum_{ij}^{L} e^{\imath k(r_i-r_j)}\langle B_i B_j\rangle$, where $B_i = \mathbf{S}_i \cdot \mathbf{S}_{i+1}$ denotes the bond operator. See Fig. 5 for example of $M_d(k)$ data. Staggered dimerization $\epsilon(x)$, introduced in (B7), represent low-energy limit of the staggered part of the bond operator, $B_i \to \mathcal{B}(x) + (-1)^x\epsilon(x)$, while its uniform part $\mathcal{B}$ represents an average bond energy.

To charaterize distinct phases in the phase diagram, we first show examples of both spin and dimer structure factors of the systems with length $L = 1600$ in Fig. 5.

A. "N^z" phase

The "N^z" phase is well understood for the case $\Delta > 1$ without DM interaction. A finite DM interaction pushes the phase boundary to lower Δ value due the renormalization of the effective anisotropy, which can be seen in the phase diagram. Fig. 5(a) plots the structure factors at $\Delta = 1.1$, $D/J = 0.1$, and $h/J = 0.2$, where the structure factor $M_s^z(k)$ shows a clear peak at commensurate momentum $k = \pi$, indicating the presence of the Nèel Ising order. On the contrary, the structure factor $M_s^y(k)$ has two smaller peaks, one at commensurate momentum $k = \pi$ and another at incommensurate momentum $k = k^\star < \pi$. However, since both peaks in the

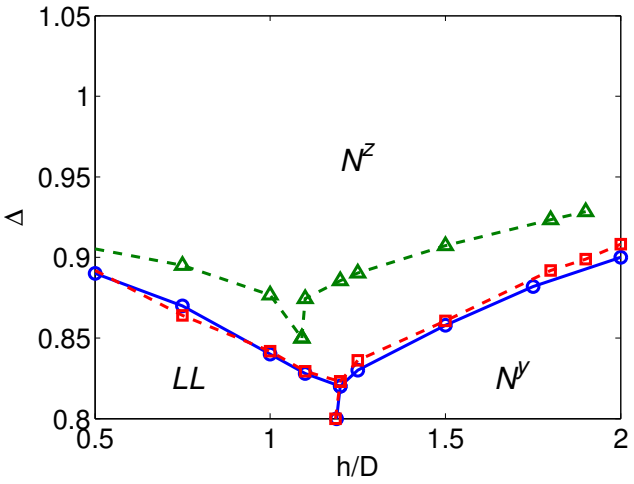

FIG. 4: (Color online) The ground state phase diagram of the system in Eq.(1) at $D/J = 0.1$ as determined by DMRG (open circles) and iTEBD (open squares) calculations for system with L=1200 sites. For comparison, the phase diagram at $D/J = 0.05$ is also provided obtained by DMRG simulation for system with $L = 800$ sites (open triangles). The lines are guides to eye.

$M_s^y(k)$ structure factor are substantially smaller than the peak in $M_s^z(k)$ at commensurate $k = \pi$, we conclude that at this point the spin chain is the "N^z" phase, with no "N^y"-kind Ising order.

B. "N^y" phase

When Δ is small while h is sufficient large, the system enters into the "N^y" phase. This phase is characterized by a dominant peak of the structure factor $M_s^y(k)$ at commensurate momentum $k = \pi$, while peaks in $M_s^z(k = \pi)$ and $M_s^y(k = k^\star)$ are much smaller, see Fig. 5(b). Note that the "N^y" Néel Ising order, which is also present in the system without DM interaction, is suppressed by the finite DM interaction, especially for $h \leq D$. See Appendix D for the analytical explanation of this.

C. LL phase

The system is in the LL phase when both Δ and h are smal enough, and is characterized by the dominant peak in the structure factor $M_s^y(k)$ at the incommensurate momentum $k = k^\star < \pi$ as shown in Fig. 5(c). For example, the peak is at $k^* \approx 0.965\pi$ for $\Delta = 0.7$, $D/J = 0.1$, and $h/J = 0.075$. For the same set of parameters, the field theory predicts the peak to be at $k = \pi \pm t_\varphi$, with $t_\varphi = \sqrt{h^2 + D^2}/(\pi J/2)$, see (B11) and (E22). This prediction translates into $k^* = 0.975\pi$, which is consistent with the numerical result. Notice that our numerical

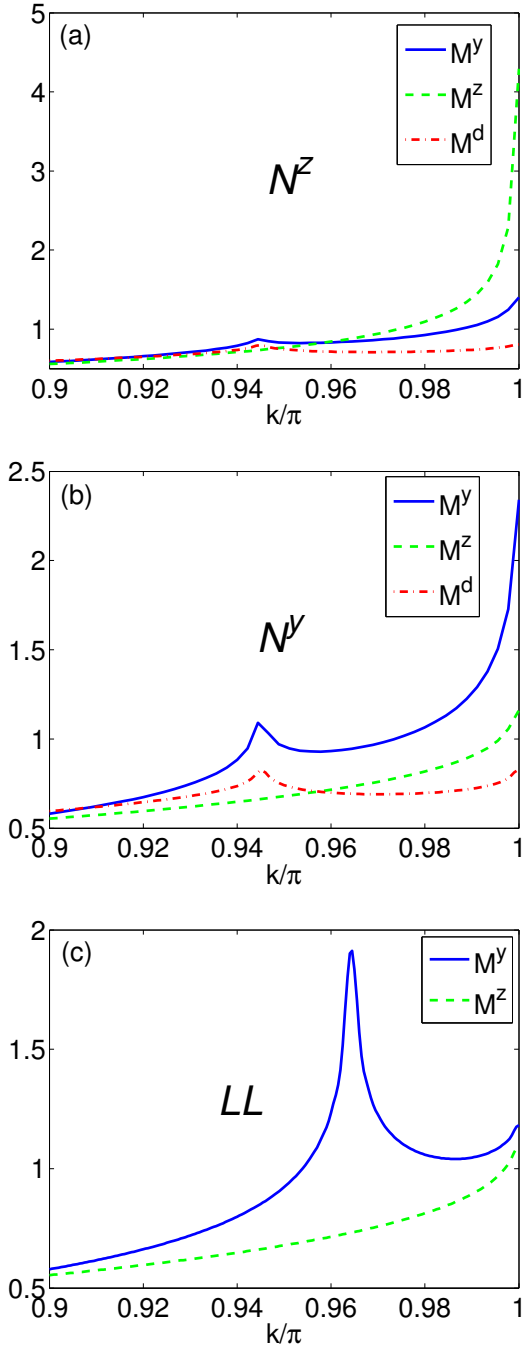

FIG. 5: (Color online) Structure factors M_s^y (blue solid line), M_s^z (green dashed line) with $L = 1600$ and M_d (red dash-dot line) with $L = 1200$ (a) in the N^z phase at $\Delta = 1.1$, $D/J = 0.1$, $h/J = 0.2$, (b) in the N^y phase at $\Delta = 0.7$, $D/J = 0.1$, $h/J = 0.2$, and (c) in the LL phase at $\Delta = 0.7$, $D/J = 0.1$, $h/J = 0.075$.

calculations give a slightly smaller k^*, which is caused by the difference of spinon velocity v from the zero field value $\pi J/2$ and finite-size effects. Similar with $M_s^y(k)$, the dimer structure factor also exhibits a two-peak fea-

ture at both commensurate $k = \pi$ and incommensurate momentum $k = k^\star < \pi$. This is direct consequence of the chiral rotation (B1) which 'mixes up' staggered magnetization and dimerization operators as equations (B7) and (B5) (equivalently, (12)) show.

Having characterized the distinct phases, now we can try to determine the phase boundary between them.

D. "N^y"-"N^z" boundary

The phase boundary between the two Ising phases is determined by the order parameters $N^y(\pi)$ and $N^z(\pi)$, which should saturate to a finite nonzero value in the thermodynamic limit in the "N^y" and "N^z" phase, correspondingly, and vanish elsewhere. Unfortunately, due to large finite size effects (see Section V for details), the order parameters tend to behave continuously across the anticipated phase boundary, even though their values in the "wrong" phase become very small. We therefore try to identify the phase boundary by looking for the crossing point where the two order parameters take the same value since the "N^z" Ising order dominates at larger Δ while the "N^y" order wins at smaller Δ. Example of determining the phase boundary in this way is shown in Fig. S1(a) in the Appendix F.

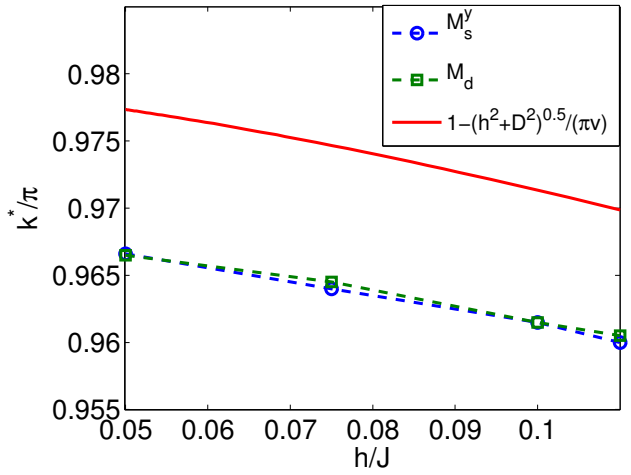

FIG. 6: (Color online) The dependence of the incommensurate peak momentum $k^\star$ in the spin structure factor $M_s^y(k)$ (blue dots) and dimer structure factor $M_d(k)$ (green squares) as a function of the transverse magnetic field h at $D/J = 0.1$. Red line denotes the theoretical prediction, we used $v = \pi J/2$.

E. LL-Ising boundary

In the LL phase all order parameters vanish in the thermodynamic limit. Unfortunately, again due to strong finite-size effects, an unambiguous identification of this phase is difficult since both Ising order parameters remain nonzero, although really small, inside it. We observe that in both "N^y" and LL phases, the spin structure factor $M_s^y(k)$ develops peaks at commensurate momentum $k = \pi$ and at incommensurate momentum $k = k^\star < \pi$, see Fig. 5. This is direct consequence of Eq.(12) and (B5) which show that $N^y \sim \cos\theta_0 \mathcal{N}^y + \sin\theta_0 \xi$. While $\mathcal{N}^y$ is peaked at *zero* momentum (which means that its contribution to spin density $S^y \sim (-1)^x N^y$ is peaked at momentum π), the rotated dimerization operator ξ is peaked at $\pm t_\varphi$, see Eq.(B9) and (B11). Therefore $M_s^y(k)$ is expected to have peaks at both $k = \pi$ *and* $k^* = \pi - t_\varphi$. Similar two-peak structure, with maxima at momenta π (coming from $\mathcal{N}^y$) and k^* (coming from ξ), shows up in the dimer structure factor $M_d(k)$, in full agreement with second line of (12). Fig. 5 (a),(b) shows corresponding numerical data.

Inside the "N^y" phase the dominant peak of M_s^y is at $k = \pi$, suggesting well developed Néel order of "N^y" kind. On the contrary, deep inside the LL phase $M_s^y(k^*)$, which comes from power-law correlations of the rotated dimerization operator ξ, dominates over the peak at π. This numerical finding is fully consistent with our low-energy bosonization calculation in Appendix E 3, Eq. (E22), which shows that spin correlations caused by rotated operators ξ and $\mathcal{N}^z$ are the slowest-decaying ones. Therefore the phase boundary between the LL and "N^y" phases can be identified from the condition $M_s^y(k = k^\star) = M_s^y(k = \pi)$. The resulting phase boundary agree well with theoretical prediction. Similarly, the boundary between the LL and "N^z" phases is determined by $M_s^y(k = k^\star) = M_s^z(k = \pi)$, see Fig. S1b. Since M_s^y shows a dominant peak at $k = k^\star$ in the LL phase while the $\mathcal{N}^z$ phase has a dominant order at $k = \pi$, the phase boundary between these two phases can be determined by the crossing point of the above quantities.

Further quantitative agreement can be established by comparing numerical data for $k^\star$, extracted from $M_s^y(k)$ and $M_d(k)$ data, with the analytical prediction $k^* = \pi - t_\varphi = \pi - \sqrt{D^2 + h^2}/v$, as shown in Fig. 6. Small difference between the measured and the predicted k^* values is probably due to our omission of the velocity renormalization by marginal operators.

Finally, we have also calculated the phase diagram of the system with smaller DM interaction $D/J = 0.05$. The phase diagram for $L = 800$ chain is shown in Fig. 4 by a green dashed line. Compared with larger DM interaction $D/J = 0.1$ case, the phase boundaries for both N^z-LL and N^z-N^y phase transitions move to higher Δ values, in qualitative agreement with theoretical expectations – see phase diagrams in Figs. 2 and 3 for a similar comparison.

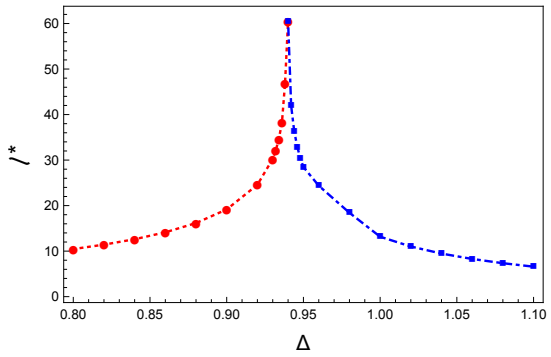

FIG. 7: (Color online) Plot of the critical RG ℓ^* for which $|y_c(\ell^*)| = 1$ (obtained by solving KT equations, see Appendix C) as a function of the XXZ anisotropy Δ. Here $D/J = 0.1$ and $h/J = 0.2$. The system is in the "N^y" phase (red line) for $\Delta < \Delta_c \simeq 0.94$ (the phase boundary Δ_c is determined from Eq. (15)), while at $\Delta > \Delta_c$ the system enters "N^z" phase (blue line). Near the transition point, $\ell^* \gg \ell_s = 7.37$.

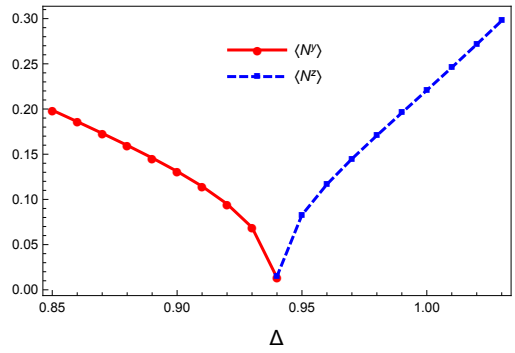

FIG. 8: (Color online) Order parameters as a function of Δ for two ordered states "N^y" and "N^z", at $D/J = 0.1$, $h/J = 0.2$, and RG length scale $\ell = \ell_s$. Here Δ is near the phase boundary $\Delta_c \simeq 0.94$ (determined from Eq. (15)). See main text and Appendix E for details.

V. ANALYTICAL UNDERSTANDING OF FINITE SIZE EFFECTS IN DMRG STUDY

Our formulation provides convenient way to understand some of the finite size effects unavoidable in numerical study of the problem. Here we focus on the case of relatively strong DM interaction $D/J = 0.1$, analytical and numerical phase diagrams for which are presented in Fig. 2 and Fig. 4, correspondingly.

By solving the RG equations (10) we obtain the critical RG scale ℓ^* at which the order develops fully, namely $|y_C(\ell^*)| = 1$. We find that ℓ^* grows rapidly as Δ is approaching the phase boundary between "N^y" and "N^z" states, as shown in Fig. 7, with $\ell \approx 50$ near the critical point. However the finite size of the system used in the DMRG study, $L = 1600$ in units of the lattice spacing a, corresponds to a much smaller RG scale of $\ell_s = \ln[1600] = 7.37$. Therefore the RG scales greater than ℓ_s are *not accessible* for DMRG. In other words, if we associate the correlation length $\xi = ae^{\ell^*}$ with the order which develops at ℓ^*, and if it happens that $\ell^* > \ell_s = 7.37$, than the DMRG simulations will not be sensitive to the development of the long-range order in this case. This is the basic explanation of the unavoidable difficulty one encounters in numerical determination of the phase boundaries between various phases.

In addition to calculating ℓ^* associated with the development of long-range order, we can also calculate the order parameters for "N^y" and "N^z" phases developing in the system as functions of the running RG scale ℓ. Appendix E describes how it is done. We show there that the required order parameters are given by

$$\langle N^y \rangle = \langle \mathrm{Re}[e^{i\beta\vartheta/2}] \rangle, \quad \langle N^z \rangle = \langle \mathrm{Im}[e^{i\beta\vartheta/2}] \rangle. \qquad (18)$$

Eq. (E18) shows explicit form of the order parameters in terms of running couplings $y_{C,\sigma}(\ell)$. Fig. 8 illustrates our results. It shows the order parameters $\langle N^{y,z} \rangle$ which are evaluated at the maximum possible for our chain RG scale $\ell = \ell_s$. Observe that in agreement with the numerical data in Fig. S1a, there is a noticeable asymmetry between these two order parameters: the order parameter of the "N^y" phase is smaller than that of the "N^z" phase.

VI. CONCLUSIONS

Extensive DMRG study shows an excellent agreement with analytical investigation based on the RG analysis of weakly perturbed Heisenberg chain. We have worked out full phase diagram of the model in the $\Delta - (h/D)$ plane. Our numerical findings match predictions of Ref. 16 well, and confirm the prevalence of "N^z" Néel Ising order in the regime of comparable Dzyaloshinskii-Moriya (DM) and magnetic field magnitudes[15]. In addition, we find that significant finite-size corrections observed numerically are well explained by the 'logarithmic slowness' of the KT RG flow. As a result of that very large RG scales ℓ^*, far exceeding those set by the finite length L of the chain used in DMRG, are required for reaching the Ising-ordered phases.

Our numerical data also confirms the existence of the critical Luttinger liquid phase with fully broken spin-rotational invariance. This phase with dominant incommensurate spin and dimerization power-law correlations is a quantum analogue of the classical chiral soliton lattice.

Our findings open up a possibility of the experimental check of theoretical predictions in quasi-one-dimensional antiferromagnets with a uniform DM interaction[13,14]. The idea is to probe the spin correlations at a finite temperature above the critical ordering temperature of the material when inter-chain spin correlations, which drive the three-dimensional ordering, are not important while individual chains still possess sufficient for exper-

imental detection anisotropy of spin correlations caused by the uniform DM interaction. Under these conditions one should be able to probe the fascinating competition between the uniform DM interaction and the transverse external magnetic field.

Acknowledgments

O.A.S. would like to thank I. Affleck for several discussions related to this work. W.J. and O.A.S. are supported by the National Science Foundation grant NSF DMR-1507054. H.C.J was supported by the Department of Energy, Office of Science, Basic Energy Sciences, Materials Sciences and Engineering Division, under Contract DE-AC02-76SF00515. Y.-H. C. is supported by a Thematic Project at Academia Sinica.

Appendix A: Bosonization

The low-energy description is provided by the parameterization[15] $\boldsymbol{S}(x) \approx \boldsymbol{J}(x) + (-1)^n \boldsymbol{N}(x)$, where $\boldsymbol{J} = \boldsymbol{J}_L + \boldsymbol{J}_R$, and $\boldsymbol{J}_L(x)$ and $\boldsymbol{J}_R(x)$ are the uniform left- and right-moving spin currents, and $\boldsymbol{N}(x)$ is the staggered magnetization (our order parameter). Here $x = na$ in terms of lattice constant a. These fields are expressed in terms of bosonic fields (ϕ, θ) (this expansion is not specific to the SU(2), Heisenberg, point and can be generalized easily to a more general XXZ Hamiltonian).

$$\begin{aligned} J^+_R = \frac{1}{2\pi a} e^{-i\sqrt{2\pi}(\phi-\theta)},\ J^+_L = \frac{1}{2\pi a} e^{i\sqrt{2\pi}(\phi+\theta)}, \\ J^z_R = \frac{\partial_x\phi - \partial_x\theta}{2\sqrt{2\pi}},\ J^z_L = \frac{\partial_x\phi + \partial_x\theta}{2\sqrt{2\pi}}, \end{aligned} \tag{A1}$$

and

$$\boldsymbol{N} = A(-\sin[\sqrt{2\pi}\theta],\ \cos[\sqrt{2\pi}\theta],\ -\sin[\sqrt{2\pi}\phi]). \tag{A2}$$

Here, $A \equiv \gamma/(\pi a_0)$, and $\gamma = \langle \cos(\sqrt{2\pi}\phi_\rho)\rangle \sim O(1)$ is determined by gapped charged modes of the chain. The Hamiltonian in Eq. (1) is approximated in low energy limit as[15,16,19]

$$H = H_0 + V + H_{\rm bs}, \tag{A3}$$

where

$$\begin{aligned} H_0 &= \frac{2\pi v}{3}\int \mathrm{d}x(\boldsymbol{J}_R\cdot\boldsymbol{J}_R + \boldsymbol{J}_L\cdot\boldsymbol{J}_L), \\ V &= -D\int \mathrm{d}x(J^z_R - J^z_L) - h\int \mathrm{d}x(J^x_R + J^x_L), \\ H_{\rm bs} &= -g_{\rm bs}\int \mathrm{d}x[J^x_R J^x_L + J^y_R J^y_L + (1+\lambda)J^z_R J^z_L], \end{aligned} \tag{A4}$$

where λ is the total XXZ anisotropy described by Eq. (7).

Appendix B: Chiral rotation

The system Hamiltonian is described in Eq. (A4). It is convenient to exploit the extended symmetry of H_0 and treat both vector perturbations h and D equally by performing a chiral rotation of spin currents about the y axis[15,16,19]

$$\boldsymbol{J}_{R/L} = \mathcal{R}(\theta_{R/L})\boldsymbol{M}_{R/L}, \tag{B1}$$

with $\boldsymbol{M}_{R/L}$ is the spin current in the rotated frame, and $\mathcal{R}$ is the rotation matrix,

$$\mathcal{R}(\theta_{R/L}) = \begin{pmatrix} \cos\theta_{R/L} & 0 & \sin\theta_{R/L} \\ 0 & 1 & 0 \\ -\sin\theta_{R/L} & 0 & \cos\theta_{R/L}. \end{pmatrix}, \tag{B2}$$

where

$$\theta_R = \theta_0 + \pi/2,\ \theta_L = -\theta_0 + \pi/2,\ \theta_0 \equiv \arctan\left(\frac{-D}{h}\right). \tag{B3}$$

Via this chiral rotation, vector perturbation V in Eq. (A4) becomes

$$\begin{aligned} V &= -\sqrt{D^2+h^2}\int \mathrm{d}x(M^z_R + M^z_L) \\ &= -\frac{\sqrt{D^2+h^2}}{\sqrt{2\pi}}\int \mathrm{d}x\partial_x\varphi. \end{aligned} \tag{B4}$$

The staggered magnetization transforms as

$$\boldsymbol{N} = (-\mathcal{N}^z, \cos\theta_0\mathcal{N}^y + \sin\theta_0\xi, \mathcal{N}^x), \tag{B5}$$

Here $\boldsymbol{\mathcal{N}}$ and ξ denote the *staggered magnetization* and *dimerization* in the rotated frame. They, as well as rotated spin currents $\boldsymbol{M}_{R/L}$, are expressed in terms of of abelian bosonic fields φ and ϑ. Staggered magnetization $\mathbf{N}$ in (A2), staggered dimerization $\epsilon = (\gamma/\pi a_0)\cos[\sqrt{2\pi}\phi]$ and spin currents $\boldsymbol{J}_{R/L}$ are written in terms of (ϕ,θ) pair as Eq. (A1) and (A2) show. Therefore, in the rotated frame

$$\boldsymbol{\mathcal{N}} = \frac{\gamma}{\pi a_0}(-\sin\sqrt{2\pi}\vartheta, \cos\sqrt{2\pi}\vartheta, -\sin\sqrt{2\pi}\varphi) \tag{B6}$$

and $\xi = (\gamma/\pi a_0)\cos\sqrt{2\pi}\varphi$.

Relation (B5) is obtained by observing that chiral rotation (B1) of vector currents corresponds to the following rotation of Dirac spinors[16,31] $\Psi_{R/L,s} = e^{-i\theta_{R/L}\sigma^y/2}\tilde{\Psi}_{R/L,s}$ in terms of which spin currents are expressed[22] as $J^a_{R/L} = \Psi^+_{R/L}\sigma^a\Psi_{R/L}/2$ and $M^a_{R/L} = \tilde{\Psi}^+_{R/L}\sigma^a\tilde{\Psi}_{R/L}/2$. The (original) staggered magnetization, $N^a = (\Psi^+_R\sigma^a\Psi_L + \Psi^+_L\sigma^a\Psi_R)/2$, rotates into (B5). Similarly, staggered dimerization $\epsilon(x) \sim (-1)^{x/a}\mathbf{S}(x)\cdot\mathbf{S}(x+a)$ transforms as

$$\epsilon = \cos\theta_0\xi - \sin\theta_0\mathcal{N}^y. \tag{B7}$$

Rotation (B1) transforms backscattering Hamiltonian in (A4) into,

$$H_{\rm bs} = 2\pi v \int {\rm d}x \Big[\sum_\alpha y_\alpha M_R^\alpha M_L^\alpha + \\ + y_A (M_R^z M_L^x - M_R^x M_L^z) \Big], \tag{B8}$$

where $\alpha = x, y, z$ and the initial values of coupling constants y_α and y_A are shown in Eq. (5).

We see from Eq. (B4) that in the rotated frame the chain experiences an external magnetic field $h_{\rm eff} \equiv \sqrt{D^2 + h^2}$ applied along z-axis. This term is then absorbed into the isotropic Hamiltonian H_0 by the position-dependent shift

$$\varphi \to \varphi + t_\varphi x, \quad t_\varphi \equiv \sqrt{D^2 + h^2}/v = h_{\rm eff}/v. \tag{B9}$$

As a result of this shift, the spin currents, the staggered magnetization and the dimerization in the rotated frame are modified as

$$M_R^+ \to M_R^+ e^{-it_\varphi x}, \quad M_L^+ \to M_L^+ e^{it_\varphi x}, \\ M_R^z \to M_R^z + \frac{t_\varphi}{4\pi}, \quad M_L^z \to M_L^z + \frac{t_\varphi}{4\pi}, \tag{B10}$$

and

$$\mathcal{N}^z \to -\frac{\gamma}{\pi a_0} \sin(\sqrt{2\pi}\varphi + t_\varphi x), \\ \xi \to \frac{\gamma}{\pi a_0} \cos[\sqrt{2\pi}\varphi + t_\varphi x]. \tag{B11}$$

The φ field shift (B9) will also transform the expression for the chain backscattering (B8) to Eq. (3), in which we neglected additional small terms coming from the shifts in $M_{R/L}^z$.

Appendix C: Analytical solution of Kosterlitz-Thouless (KT) equations

Analytical solution of the Kosterlitz-Thouless (KT) equations in Eq. (10) is given by

$$y_\sigma(l) = \begin{cases} \mu \dfrac{y_\sigma(0)\cosh(\mu l) - \mu \sinh(\mu l)}{-y_\sigma(0)\sinh(\mu l) + \mu \cosh(\mu l)}, & C > 0, \\ \mu \dfrac{y_\sigma(0)\cos(\mu l) + \mu \sin(\mu l)}{-y_\sigma(0)\sin(\mu l) + \mu \cos(\mu l)}, & C < 0. \end{cases} \tag{C1}$$

with $\mu = \sqrt{|C|}$. Also,

$$y_C(l) = {\rm sign}(y_C(0)) \sqrt{y_\sigma(l)^2 - C}. \tag{C2}$$

The sign of $y_C(l)$ depends on the sign of its initial value. The critical ℓ^*, at which $|y_C(l = l^*)| = 1$, can be determined by Eq. (C1) and (C2), and is shown is Fig. 7.

Appendix D: XXZ model in transverse field, $D = 0$

If we set $D = 0$, two rotation angles $\theta_R = \theta_L = \pi/2$, and $\theta^- = 0$. Then $y_A(0) = 0$. In this condition, our model Hamiltonian (1) reduces to a XXZ model in a uniform transverse field. The RG equations for the backscattering are,

$$\frac{dy_x}{dl} = y_y y_z, \quad \frac{dy_y}{dl} = y_x y_z, \quad \frac{dy_z}{dl} = y_x y_y, \tag{D1}$$

and the initial values are,

$$y_x(0) = -\frac{g_{\rm bs}}{2\pi v}[1 + \lambda], \; y_y(0) = y_z(0) = -\frac{g_{\rm bs}}{2\pi v}, \tag{D2}$$

It is easy to find that $y_y(\ell) = y_z(\ell)$ for all ℓ so that the RG equations above again acquire a KT form. Now $\lambda = c(1 - \Delta)$ so that we obtain

$$y_C(0) = -\frac{g_{\rm bs}}{4\pi v}\lambda, \; y_\sigma(0) = \frac{g_{\rm bs}}{2\pi v}, \; C = (\frac{g_{\rm bs}}{2\pi v})^2 (1 - \frac{\lambda^2}{4}). \tag{D3}$$

Using Eq. (C1), we find

$$y_\sigma(\ell) = 2\mu \frac{y_C^2/(y_\sigma + \mu)^2}{e^{-2\mu\ell} - y_C^2/(y_\sigma + \mu)^2}, \tag{D4}$$

where $y_{C/\sigma}$ in the right-hand-side are those at $\ell = 0$ (their initial values). Therefore, since $y_\sigma(0) = g_{\rm bs}/(2\pi v) > \mu = \sqrt{y_\sigma^2 - y_C^2}$, there is a divergence, signaling strong-coupling limit, at $\ell_{\rm div} \approx \mu^{-1} \ln\big[4|\lambda|^{-1}\big]$. Observe that $\ell_{\rm div}$ is finite for any $\Delta \neq 1$, meaning that the two ordered phases are separated by the critical LL one, which is just an isotropic Heisenberg chain in a magnetic field.

For $\Delta < 1$, we have $\lambda > 0$, $y_C(0) < 0$, and then $y_C(l) \to -\infty$, which leads to the "N^y" state. For $\Delta > 1$, instead $\lambda < 0$ and $y_C(0) > 0$, so that $y_C(l) \to +\infty$, hence one obtains the "N^z" state. These two phases are separated by the critical line at $\Delta = 1$. Our phase diagrams in Figs. 3 and 2 display exactly this behavior: setting $D = 0$ places the model at $h/D \to \infty$, where the critical line separating the two Ising states approaches horizontal asymptote at $\Delta = 1$.

The above argument agrees with Ref.[24], which studied the ground state of the following Hamiltonian,

$$\mathcal{H} = \sum_j \left[J(S_j^x S_{j+1}^x + S_j^y S_{j+1}^y + \Delta S_j^z S_{j+1}^z) - h S_j^x \right]. \tag{D5}$$

It was found that for $h \neq 0$ spectrum is gapped for both $\Delta > 1$ and $\Delta < 1$[24]. The Ising order that develops is of "N^z" ("N^y") kind for $\Delta > 1$ ($\Delta < 1$). Our RG equations evidently capture this physics well.

Appendix E: Calculation of the order parameter

In Ref. 32 Lukyanov and Zamolodchikov have suggested a general expression for the expectation value of

the vertex operator $\langle e^{ia\vartheta}\rangle$, see Eq.(20) in that reference, of the sine-Gordon model given by the action

$$S_{sG} = \int d^2x \Big\{ \frac{1}{16\pi}(\partial_\nu \vartheta)^2 - 2\mu\cos(\beta'\vartheta)\Big\}. \tag{E1}$$

Their conjecture is as follows (for $\beta'^2 < 1$, and $|\mathrm{Re}\ a| < 1/(2\beta')$, which are required for the convergence) ,

$$\langle e^{ia\vartheta}\rangle = \Big[\frac{m\Gamma(\frac{1}{2}+\frac{\xi}{2})\Gamma(1-\frac{\xi}{2})}{4\sqrt{\pi}}\Big]^{2a^2} \exp\Big\{\int_0^\infty \frac{dt}{t}\Big[\frac{\sinh^2(2a\beta' t)}{2\sinh(\beta'^2 t)\sinh(t)\cosh\big((1-\beta'^2)t\big)} - 2a^2 e^{-2t}\Big]\Big\}, \tag{E2}$$

where

$$m = 2M\sin(\pi\xi/2), \quad \xi = \frac{\beta'^2}{1-\beta'^2} \tag{E3}$$

and M is the soliton mass.

1. Perturbation H_C and H_σ

Here we work out the action for our KT Hamiltonian by considering H_C and H_σ as perturbations to the harmonic Hamiltonian H_0. Provided that the field is small enough, so that the scaling dimensions of various operators are given by their values at the Heisenberg point, we have

$$\begin{aligned} M^z_R &= \frac{1}{2\sqrt{2\pi}}(\partial_x\varphi - \partial_x\vartheta), \\ M^z_L &= \frac{1}{2\sqrt{2\pi}}(\partial_x\varphi + \partial_x\vartheta). \end{aligned} \tag{E4}$$

and therefore

$$\begin{aligned} H_\sigma &= -\frac{v y_\sigma}{4}\int \mathrm{d}x[(\partial_x\varphi)^2 - (\partial_x\vartheta)^2], \\ H_C &= \frac{v y_C}{2\pi a^2}\int \mathrm{d}x\cos(2\sqrt{2\pi}\vartheta). \end{aligned} \tag{E5}$$

Therefore, the action, which determines the partition function $Z = \int e^{-S}$, is

$$\begin{aligned} S = \int \mathrm{d}x\mathrm{d}\tau\Big\{ &-i\partial_x\vartheta\partial_\tau\varphi + \frac{1}{2}[v_1(\partial_x\varphi)^2 + v_2(\partial_x\vartheta)^2] \\ &+ \frac{v y_C}{2\pi a^2}\cos(\sqrt{8\pi}\vartheta)\Big\}. \end{aligned} \tag{E6}$$

where

$$v_1 = v(1-\frac{y_\sigma}{2}), \quad v_2 = v(1+\frac{y_\sigma}{2}). \tag{E7}$$

We integrate out the φ field using duality $\partial_x\vartheta\partial_\tau\varphi = \partial_x\varphi\partial_\tau\vartheta$ and then the action factorizes

$$\begin{aligned} S = \int \mathrm{d}x\mathrm{d}\tau\Big\{ &\frac{v_1}{2}(\partial_x\varphi - \frac{i}{v_1}\partial_\tau\vartheta)^2 + \frac{1}{2v_1}(\partial_\tau\vartheta)^2 + \frac{v_2}{2}(\partial_x\vartheta)^2 \\ &+ \frac{v y_C}{2\pi a^2}\cos(\sqrt{8\pi}\vartheta)\Big\}. \end{aligned} \tag{E8}$$

The first, φ-dependent piece in Eq. (E6) is integrated away. The remaining ϑ part of the action is

$$\begin{aligned} S_\vartheta \ = \ &\int \mathrm{d}x dy\Big\{\frac{1}{2}\sqrt{\frac{v_2}{v_1}}((\partial_x\vartheta)^2 + (\partial_\tau\vartheta)^2) \\ &+ \frac{y_C}{2\pi a^2}\frac{v}{u}\cos(\sqrt{8\pi}\vartheta)\Big\}, \end{aligned} \tag{E9}$$

with $y = u\tau$ and set $u = \sqrt{v_1 v_2}$. Finally we rescale ϑ,

$$\vartheta = \frac{1}{\sqrt{8\pi}}\Big(\frac{v_1}{v_2}\Big)^{\frac{1}{4}}\tilde{\vartheta}, \tag{E10}$$

and arrive at the desired form of Eq. (E1),

$$S_\vartheta = \int d^2x\Big\{\frac{1}{16\pi}(\partial_\nu\tilde{\vartheta})^2 - 2\mu\cos(\tilde{\beta}\tilde{\vartheta})\Big\}, \tag{E11}$$

where

$$\mu \equiv \frac{|y_C|}{4\pi a^2}\frac{v}{u}, \quad \tilde{\beta} \equiv \Big(\frac{v_1}{v_2}\Big)^{\frac{1}{4}}. \tag{E12}$$

Here, for the case of $y_C > 0$, we made an additional shift $\tilde{\vartheta} \to \tilde{\vartheta} + \pi/\tilde{\beta}$ in order to change the sign of the cosine term. The case of $y_C < 0$ does not require any additional shifts, $\tilde{\vartheta} = \tilde{\vartheta}$. The parameters (E12) of the action can easily be written in terms of $y_{C,\sigma}$,

$$\begin{aligned} u = v\sqrt{1-y_\sigma^2/4}, \quad \mu = \frac{1}{4\pi a^2}\frac{|y_C|}{\sqrt{1-y_\sigma^2/4}}, \\ \tilde{\beta} = \Big(\frac{1-y_\sigma/2}{1+y_\sigma/2}\Big)^{\frac{1}{4}}. \end{aligned} \tag{E13}$$

The expectation value we intend to compute is $\langle e^{i\sqrt{2\pi}\vartheta}\rangle = \langle e^{i\tilde{\beta}\tilde{\vartheta}/2}\rangle$, and thus a in Eq. (E2) is just $a \equiv \tilde{\beta}/2$.

We observe that our order parameters are obtained as $N^y \sim \cos\sqrt{2\pi}\vartheta \propto \mathrm{Re}\langle e^{i\tilde{\beta}\tilde{\vartheta}/2}\rangle$, while $N^z \sim \sin\sqrt{2\pi}\vartheta \propto \mathrm{Im}\langle e^{i\tilde{\beta}\tilde{\vartheta}/2}\rangle$. The shift described just below Eq. (E12), which is needed for $y_C > 0$, transforms $\langle e^{i\tilde{\beta}\tilde{\vartheta}/2}\rangle$ into $e^{i\pi/2}\langle e^{i\tilde{\beta}\tilde{\vartheta}/2}\rangle$ and thus precisely corresponds to the change of the order from the "N^y" kind (realized for $y_C < 0$) to the "N^z" kind (realized for $y_C > 0$).

2. The order parameter $\langle e^{i\frac{\tilde\beta}{2}\tilde\vartheta}\rangle$

We are interested to evaluate the expectation value

$$\langle e^{i\frac{\tilde\beta}{2}\tilde\vartheta}\rangle = Ae^I, \quad A \equiv \Big[\frac{m\Gamma(\frac{1}{2}+\frac{\xi}{2})\Gamma(1-\frac{\xi}{2})}{4\sqrt{\pi}}\Big]^{\tilde\beta^2/2}. \quad \text{(E14)}$$

Here I is obtained from Eq. (E2) by setting $a=\tilde\beta/2$,

$$I \equiv \int_0^\infty \frac{dt}{t}\Big[\frac{\sinh(\tilde\beta^2 t)}{2\sinh(t)\cosh\big((1-\tilde\beta^2)t\big)} - \frac{\tilde\beta^2}{2}e^{-2t}\Big]. \quad \text{(E15)}$$

The convergence of I is easy to check: $\tilde\beta^2<1$ is required for $t\to\infty$. Using identity $\Gamma(1-x)\Gamma(x)=\pi/\sin(\pi x)$, and with m in Eq. (E3), the expression for A becomes

$$A = \Big[\frac{\sqrt{\pi}}{2}M\frac{\Gamma(\frac{1}{2}+\frac{\xi}{2})}{\Gamma(\xi/2)}\Big]^{\tilde\beta^2/2}. \quad \text{(E16)}$$

The relation between constant μ and mass M is (this is Eq.12 of Ref. 32)

$$\mu = \frac{\Gamma(\tilde\beta^2)}{\pi\Gamma(1-\tilde\beta^2)}\Big[M\frac{\sqrt{\pi}\Gamma(\frac{1}{2}+\frac{\xi}{2})}{2\Gamma(\frac{\xi}{2})}\Big]^{2-2\tilde\beta^2}. \quad \text{(E17)}$$

Using all these we obtain for the order parameter

$$\langle e^{i\frac{\tilde\beta}{2}\tilde\vartheta}\rangle = \Big[\frac{\pi\mu\,\Gamma(1-\tilde\beta^2)}{\Gamma(\tilde\beta^2)}\Big]^{\tilde\beta^2/[4(1-\tilde\beta^2)]} \times \exp\Big\{\int_0^\infty \frac{dt}{t}\Big[\frac{\sinh(\tilde\beta^2 t)}{2\sinh(t)\cosh\big((1-\tilde\beta^2)t\big)} - \frac{\tilde\beta^2}{2}e^{-2t}\Big]\Big\}. \quad \text{(E18)}$$

Note that Eq. (E18) is a function of $\tilde\beta$, which, in turn, is function of running $y_\sigma(\ell)$. It also depends on running $y_C(\ell)$, via μ dependence, see (E13). Thus (E18) allows us to evaluate the order parameter as a function of RG scale ℓ.

3. Luttinger liquid phase

The Luttinger-liquid (LL) phase of our model is characterized by $y_C=0, y_\sigma<0$ for $\ell\to\infty$, see Fig. 1. Correspondingly, its action is given by Eq. (E6) with $y_C=0$. From here it is easy to derive that the scaling dimension of the vertex operator $e^{i\sqrt{2\pi}\vartheta(x)}$ is $\Delta_\vartheta=\tilde\beta^2/2\approx(1-y_\sigma/2)/2$, while that of the dual field one $e^{i\sqrt{2\pi}\varphi(x)}$ is given by $\Delta_\varphi=1/(2\tilde\beta^2)\approx(1+y_\sigma/2)/2$. Backscattering renormalizes scaling dimensions through the RG flow of y_σ. Given that in the LL $y_\sigma<0$, we observe that $\Delta_\varphi<\Delta_\vartheta$ which signals that the correlation functions of fields $\mathcal{N}^z$ and ξ, which are written in terms of φ bosons, decay *slower* than those of fields $\mathcal{N}^x$ and $\mathcal{N}^y$, which are expressed via ϑ bosons. Moreover, due to Eq. (B11), correlations of $\mathcal{N}^z$ and ξ are *incommensurate*:

$$\langle \mathcal{N}^z(x)\mathcal{N}^z(0)\rangle \propto \langle \xi(x)\xi(0)\rangle \propto \frac{\cos[t_\varphi x]}{|x|^{2\Delta_\varphi}} \quad \text{(E19)}$$

while those of $\mathcal{N}^{x,y}$ are *commensurate*

$$\langle \mathcal{N}^{x,y}(x)\mathcal{N}^{x,y}(0)\rangle \propto \frac{1}{|x|^{2\Delta_\vartheta}}. \quad \text{(E20)}$$

Taken together with Eq. (12), which describes the relation between spin operators in the laboratory and rotated frames, these simple relations allow us to fully describe the asymptotic spin (and dimerization) correlations in the LL phase with fully broken spin-rotational symmetry

$$\begin{aligned}
&\langle S^x(x)S^x(0)\rangle \propto \frac{\cos[(\pi-t_\varphi)x]}{|x|^{2\Delta_\varphi}},\\
&\langle S^y(x)S^y(0)\rangle \propto \sin^2\theta_0\frac{\cos[(\pi-t_\varphi)x]}{|x|^{2\Delta_\varphi}} + \cos^2\theta_0\frac{(-1)^x}{|x|^{2\Delta_\vartheta}},\\
&\langle S^z(x)S^z(0)\rangle \propto \frac{(-1)^x}{|x|^{2\Delta_\vartheta}},\\
&\langle \epsilon(x)\epsilon(0)\rangle \propto \cos^2\theta_0\frac{\cos[(\pi-t_\varphi)x]}{|x|^{2\Delta_\varphi}} + \sin^2\theta_0\frac{(-1)^x}{|x|^{2\Delta_\vartheta}}.
\end{aligned} \quad \text{(E21)}$$

Due to $\Delta_\varphi<\Delta_\vartheta$, the LL phase is dominated by the incommensurate correlations of $S^{x,y}$ and ϵ fields. Their contribution to the equal time structure factor is easy to estimate by simple scaling analysis. For example, denoting $Q=\pi-t_\varphi$,

$$M_s^x(k) \propto \int dx \frac{e^{i(k-Q)x}}{|x|^{2\Delta_\varphi}} \sim |k-Q|^{2\Delta_\varphi-1}, \quad \text{(E22)}$$

where we extended limits of the integration to infinity due to convergence of the integral for $2\Delta_\varphi>0$. The divergence at $k=Q$ is controlled by $2\Delta_\varphi-1=-y_\sigma/2<0$ and is rounded in the system of finite size L. More careful calculation of $M_s^a(k)$ and $M_d(k)$ is possible[33–35], but is beyond the scope of the present study.

Appendix F: DMRG details

In this appendix, we provide details on determination of the phase diagram and finite size effects.

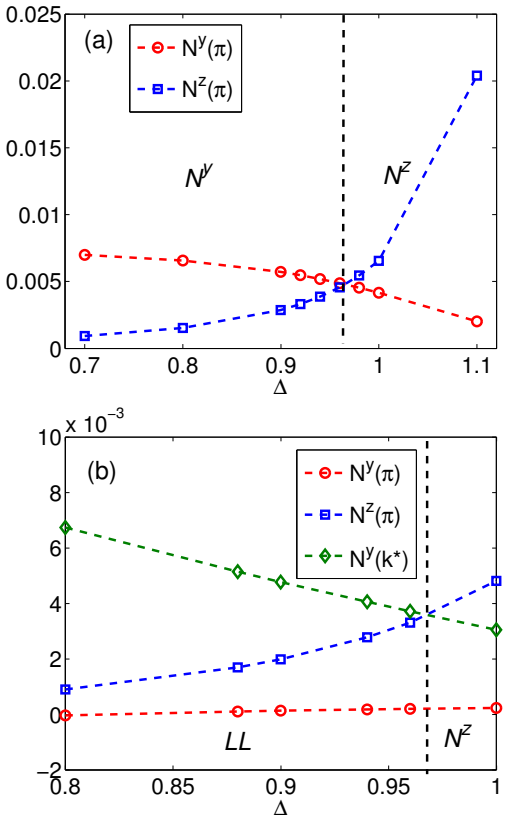

FIG. S1: (Color online) Order parameters $N^y(\pi)$ (red dots), $N^z(\pi)$ (blue squares) and $N^y(k^*)$ (green diamonds) extrapolated by a second order polynomial (17) using data from $L = 600$, 800, 1000, 1200, and 1600 chains as a function of Δ at (a) $h/J = 0.2$ and (b) $h/J = 0.05$ with $D/J = 0.1$. The crossing points of the order parameters determine the phase boundary.

1. Determination of phase boundaries

Here we describe how we determine phase boundaries numerically. In Fig. S1(a) we show the extrapolated order parameters at $k = \pi$ near phase boundary between "N^y" and an "N^z" phases. Here we can see that these two distinct orders are dominant in the corresponding phases, hence the phase boundary between them can be determined by their crossing point.

Fig. S1(b) shows the order parameters near the boundary between the LL and N^z phases, where both order parameters $N^y(k = k^*)$ and $N^z(k = \pi)$ are finite and dominant on the opposite sides of the figure, while $N^y(k = \pi)$ is vanishingly small. Notice that due to large finite-size effect, the order parameter $N^y(k = k^*)$, which should vanish after extrapolation to the thermodynamic limit $L \to \infty$, still remains finite in our L = 1600 chain although rather small. As a result, we use it to identify the LL phase as described in the main text.

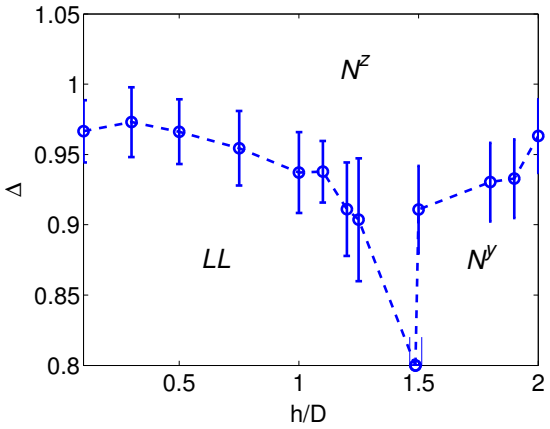

FIG. S2: (Color online) Phase diagram of the chain with $D/J = 0.1$ after the finite-size extrapolation of the order parameters to $L = \infty$ using Eq.(17). The error bar are plotted at the 95% confidence interval of the order parameters.

2. Finite size effects on the phase boundary

To check the finite-size effect on phase boundaries, we have compared phase diagrams for the chain of length $L = 1200$ calculated by DMRG and iTEBD methods as shown in Fig. 4. To minimize the boundary effect, the order parameters are calculated within the central half of the system, i.e., 600 sites in the middle of the system. We keep the same bond-link dimension and considering the same lengths for the calculation of correlation functions using iTEBD and DMRG methods. The agreement between DMRG and iTEBD results is quite good, suggesting that DMRG results are only subject to the finite size effect while the effect of open boundaries is negligible.

Fig. S2 shows phase diagram obtained by extrapolating order parameters to $L = \infty$ using second-order polynomial functions of $1/\sqrt{L}$, Eq. (17). Comparing it to the phase diagram in Fig. 4 for the finite system of size $L = 1200$, we observe the shift of N^z-LL and N^z-N^y boundaries to slightly larger Δ values. A more detailed analysis suggests that error bars associated with the finite-size extrapolation to $L = \infty$ are within 95% confidence interval, which means that our conclusion about "N^z" Ising order extending to $\Delta < 1$ region is well justified.

It is also possible to determine the phase boundary by computing the Binder cumulant,[36–38] which is widely used in Monte Carlo studies and has also been recently applied in the DMRG study[37,38]. Our preliminary investigation suggests that the phase boundary determined with the help of Binder cumulant is fully consistent with the results obtained in this work.

[1] J. Alicea, Reports on Progress in Physics **75**, 076501 (2012), URL http://stacks.iop.org/0034-4885/75/i=7/a=076501.

[2] A. Manchon, H. C. Koo, J. Nitta, S. M. Frolov, and R. A. Duine, Nat Mater **14**, 871 (2015), ISSN 1476-1122, review, URL http://dx.doi.org/10.1038/nmat4360.

[3] A. Y. Kitaev, Physics-Uspekhi **44**, 131 (2001), URL http://stacks.iop.org/1063-7869/44/i=10S/a=S29.

[4] A. Kitaev, Annals of Physics **321**, 2 (2006), ISSN 0003-4916, january Special Issue.

[5] I. E. Dzyaloshinskii, Journal of Physics and Chemistry of Solids **4**, 241 (1958), ISSN 0022-3697, URL http://www.sciencedirect.com/science/article/pii/0022369758900763.

[6] T. Moriya, Phys. Rev. **120**, 91 (1960), URL https://link.aps.org/doi/10.1103/PhysRev.120.91.

[7] I. E. Dzyaloshinskii, Sov. Phys. - JETP **20**, 665 (1965).

[8] A. Zheludev, S. Maslov, G. Shirane, Y. Sasago, N. Koide, and K. Uchinokura, Phys. Rev. B **57**, 2968 (1998), URL https://link.aps.org/doi/10.1103/PhysRevB.57.2968.

[9] Y. Togawa, T. Koyama, K. Takayanagi, S. Mori, Y. Kousaka, J. Akimitsu, S. Nishihara, K. Inoue, A. S. Ovchinnikov, and J. Kishine, Phys. Rev. Lett. **108**, 107202 (2012), URL https://link.aps.org/doi/10.1103/PhysRevLett.108.107202.

[10] S.-W. Cheong and M. Mostovoy, Nat Mater **6**, 13 (2007), ISSN 1476-1122, URL http://dx.doi.org/10.1038/nmat1804.

[11] J. Kishine and A. Ovchinnikov, Solid State Physics **66**, 1 (2015), ISSN 0081-1947, URL http://www.sciencedirect.com/science/article/pii/S0081194715000041.

[12] K. Y. Povarov, A. I. Smirnov, O. A. Starykh, S. V. Petrov, and A. Y. Shapiro, Phys. Rev. Lett. **107**, 037204 (2011), URL https://link.aps.org/doi/10.1103/PhysRevLett.107.037204.

[13] M. Hälg, W. E. A. Lorenz, K. Y. Povarov, M. Månsson, Y. Skourski, and A. Zheludev, Phys. Rev. B **90**, 174413 (2014), URL http://link.aps.org/doi/10.1103/PhysRevB.90.174413.

[14] A. I. Smirnov, T. A. Soldatov, K. Y. Povarov, M. Hälg, W. E. A. Lorenz, and A. Zheludev, Phys. Rev. B **92**, 134417 (2015), URL http://link.aps.org/doi/10.1103/PhysRevB.92.134417.

[15] S. Gangadharaiah, J. Sun, and O. A. Starykh, Phys. Rev. B **78**, 054436 (2008), URL http://link.aps.org/doi/10.1103/PhysRevB.78.054436.

[16] I. Garate and I. Affleck, Phys. Rev. B **81**, 144419 (2010), URL http://link.aps.org/doi/10.1103/PhysRevB.81.144419.

[17] C. Sun and V. L. Pokrovsky, Phys. Rev. B **91**, 161305 (2015), URL https://link.aps.org/doi/10.1103/PhysRevB.91.161305.

[18] V. E. Dmitrienko, E. N. Ovchinnikova, S. P. Collins, G. Nisbet, G. Beutier, Y. O. Kvashnin, V. V. Mazurenko, A. I. Lichtenstein, and M. I. Katsnelson, Nat Phys **10**, 202 (2014), ISSN 1745-2473.

[19] A. P. Schnyder, O. A. Starykh, and L. Balents, Phys. Rev. B **78**, 174420 (2008), URL http://link.aps.org/doi/10.1103/PhysRevB.78.174420.

[20] W. Jin and O. A. Starykh, Phys. Rev. B **95**, 214404 (2017), URL https://link.aps.org/doi/10.1103/PhysRevB.95.214404.

[21] E. Fradkin, *Field Theories of Condensed Matter Physics* (Cambridge University Press, 2013), ISBN 9781139015509, cambridge Books Online, URL http://dx.doi.org/10.1017/CBO9781139015509.

[22] O. A. Starykh, A. Furusaki, and L. Balents, Phys. Rev. B **72**, 094416 (2005), URL http://link.aps.org/doi/10.1103/PhysRevB.72.094416.

[23] T. Giamarchi and H. Schulz, Journal de Physique **49**, 819 (1988), URL https://hal.archives-ouvertes.fr/jpa-00210759.

[24] D. V. Dmitriev, V. Y. Krivnov, and A. A. Ovchinnikov, Phys. Rev. B **65**, 172409 (2002), URL http://link.aps.org/doi/10.1103/PhysRevB.65.172409.

[25] S. R. White, Phys. Rev. Lett. **69**, 2863 (1992), URL http://link.aps.org/doi/10.1103/PhysRevLett.69.2863.

[26] S. R. White, Phys. Rev. B **48**, 10345 (1993), URL http://link.aps.org/doi/10.1103/PhysRevB.48.10345.

[27] U. Schollwöck, Rev. Mod. Phys. **77**, 259 (2005), URL http://link.aps.org/doi/10.1103/RevModPhys.77.259.

[28] G. Vidal, Phys. Rev. Lett. **91**, 147902 (2003), URL http://link.aps.org/doi/10.1103/PhysRevLett.91.147902.

[29] G. Vidal, Phys. Rev. Lett. **93**, 040502 (2004), URL http://link.aps.org/doi/10.1103/PhysRevLett.93.040502.

[30] G. Vidal, Phys. Rev. Lett. **98**, 070201 (2007), URL http://link.aps.org/doi/10.1103/PhysRevLett.98.070201.

[31] O. A. Starykh, in *Handbook of Nanophysics: Nanotubes and Nanowires*, edited by K. D. Sattler (CRC Press, 2010), chap. 30.

[32] S. Lukyanov and A. Zamolodchikov, Nuclear Physics B **493**, 571 (1997), ISSN 0550-3213, URL http://www.sciencedirect.com/science/article/pii/S0550321397001235.

[33] T. Hikihara and A. Furusaki, Phys. Rev. B **58**, R583 (1998), URL https://link.aps.org/doi/10.1103/PhysRevB.58.R583.

[34] T. Hikihara and A. Furusaki, Phys. Rev. B **69**, 064427 (2004), URL https://link.aps.org/doi/10.1103/PhysRevB.69.064427.

[35] T. Hikihara, A. Furusaki, and S. Lukyanov, ArXiv e-prints (2017), 1706.02538.

[36] A. Pelissetto and E. Vicari, Physics Reports **368**, 549 (2002), ISSN 0370-1573, URL http://www.sciencedirect.com/science/article/pii/S0370157302002193.

[37] C. G. West, A. Garcia-Saez, and T.-C. Wei, Phys. Rev. B **92**, 115103 (2015), URL https://link.aps.org/doi/10.1103/PhysRevB.92.115103.

[38] S. N. Saadatmand, B. J. Powell, and I. P. McCulloch, Phys. Rev. B **91**, 245119 (2015), URL https://link.aps.org/doi/10.1103/PhysRevB.91.245119.